

ADDING A TRANSITION REGION IN GLOBAL MHD MODELS OF THE SOLAR CORONA

V. Réville¹, S. Parenti², A. S. Brun³, A. Strugarek³, A. P. Rouillard¹, M. Velli⁴, B. Perri⁵ and R. F. Pinto³

Abstract. Global MHD simulations of the solar corona are an essential tool to investigate long standing problems, such as finding the source of coronal heating and the mechanisms responsible for the onset and propagation of coronal mass ejections. The very low atmospheric layers of the corona, are however, very difficult to model as they imply very steep gradients of density and temperature over only a few thousand kilometers. In this proceedings, we illustrate some of the benefits of including a very simple transition region in global MHD models and the differences in the plasma properties, comparing with in situ data of the Parker Solar Probe.

Keywords: Solar wind, corona, MHD

1 Introduction

The new generation of inner heliosphere exploration spacecraft, Parker Solar Probe (PSP) and Solar Orbiter, has incentivized the development of ever more precise global MHD models of the solar corona. Over the past 10 years, many progresses have been made, including for instance Alfvén wave turbulence as the main process responsible for coronal heating and solar wind acceleration (Sokolov et al. 2013; van der Holst et al. 2014; Downs et al. 2016; Réville et al. 2020). The main objective of these models is to reproduce both in situ and remote sensing measurements, hence predicting accurately the thermal structure of the corona and the solar wind acceleration process. The lowest layers of the solar atmosphere, the chromosphere and the transition region, are however very challenging to model as the density and temperature vary on orders of magnitude over very short distances, in respect of the domain size of global models. In this work, we perform two similar runs of our model WindPredict-AW (Réville et al. 2020), with and without a transition region. We compare with in situ data of the first Parker Solar Probe perihelion and compute synthetic AIA images, illustrating the differences and the benefits of the transition region in the model.

2 Run description

The two simulations are based on the setup described in (Réville et al. 2020). The coronal heating is provided by two populations of turbulent Alfvén waves (parallel and anti-parallel to magnetic field) excited from the inner boundary. Table 1 sums up all the parameters of the two simulations. In the first simulation (Run 1) the inner boundary is located at $1.005R_{\odot}$, i.e. after the transition region estimated between 1000 and 2000 km above the surface ($1.001 - 1.003R_{\odot}$). The base density is fixed at $n = 2 \times 10^8 \text{ cm}^{-3}$. The amplitude of the velocity perturbations generating Alfvén waves is 30 km/s. In the second run, we place the inner boundary conditions below the transition region, at $r = 1.0002R_{\odot}$. We increase the base density by a factor 100 compared to the first run. Although the precise profile of plasma density remains poorly known in the transition region

¹ IRAP, Université Toulouse III - Paul Sabatier, CNRS, CNES, Toulouse, France

² Université Paris-Saclay, CNRS, Institut d'Astrophysique Spatiale, 91405, Orsay, France

³ AIM, CEA, CNRS, Université Paris-Saclay, Université Paris Diderot, Sorbonne Paris Cité, F-91191 Gif-sur-Yvette, France

⁴ UCLA Earth, Planetary and Space Sciences department, CA, USA

⁵ KU Leuven, CmpA, Mathematics, Belgium

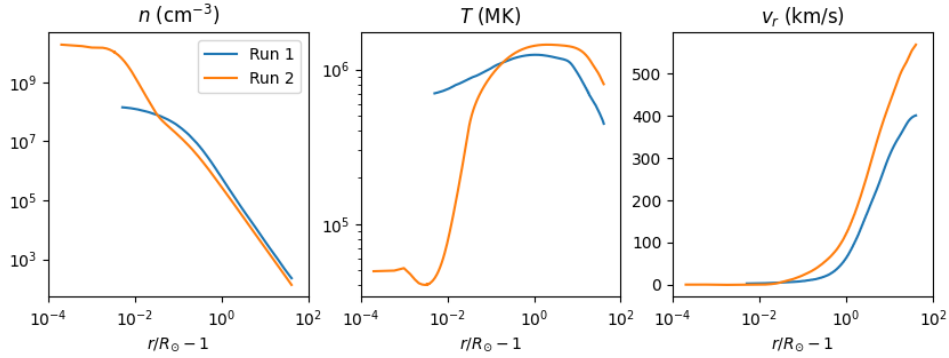


Fig. 1. Profiles of the solar wind corresponding to the source of PSP’s measurements on November 9th 2018. One can clearly see the strong density and temperature gradients corresponding to the (broadened) transition region. We see also the temperature minimum at the top of the chromosphere induced by radiative cooling.

and the chromosphere, this value is likely below expected chromospheric density. Increasing more this value does however make the simulation more difficult to run, while not changing significantly the coronal properties. The input Poynting flux is $F_w = \rho_{\odot} v_{A,r} \delta v^2$, which on average gives $\langle F_w \rangle = \sqrt{\rho_{\odot}} / 4 / \pi \langle B_{r,\odot} \rangle \delta v^2$. Both set of parameters are set to ensure that the average input Alfvén wave energy flux remain similar (see Table 1).

Run	r_{\min}	n_{\odot} (10^8 cm^{-3})	δv_{\odot} (km/s)	$\langle F_w \rangle$ ($\text{erg.cm}^{-2}/\text{s}$)	\dot{M} (M_{\odot}/yr)	Grid
1	1.005	2	30	83500	2.15×10^{-14}	196x96x192
2	1.0002	200	10	92800	2.3×10^{-14}	256x160x320

Table 1. Simulation parameters

The magnetic field at the inner boundary is kept fixed using an ADAPT magnetogram of November 6th 2018 at 12:00 UTC. This period corresponds to the first perihelion of Parker Solar Probe (see, e.g., Réville et al. 2020). It is the same for both simulations and we use a projection of this field on the first 15 spherical harmonics, which smoothes the photospheric radial field. For the second run, we had to increase the radial and angular resolution, to better resolve the strong density and temperature gradients. This is essential because the thermal conduction is aligned with the magnetic field and small numerical errors in the field direction can create strong (numerical) thermal instabilities. The global mass loss of the two simulations is reported in table 1 and is similar in both cases.

Figure 1 shows the profile of the two solar wind solutions on the path connecting PSP to the Sun on November 9th. We see the structure of the TR for Run 2 and the much stronger gradients of density and temperatures. The minimum temperature for Run 2 is around 40000K. For numerical purposes, the transition region is artificially broadened using the technique described in (Lionello et al. 2009). We see that Run 2 produces a denser, hotter, and faster wind in this coronal hole.

3 In situ data

In Figure 2, we compare the in situ measurements predicted by both models for the first perihelion of Parker Solar Probe. The red curve (Run 1) has been already published in (Réville et al. 2020). The black curve (Run 2) shares very similar properties with the red curve. The polarity of the magnetic field is very consistent in both models, which means that they predict the same sources for the solar wind. The main differences come from the predicted amplitude of wind velocities and densities. The second run shows more contrast between slow and fast wind and is generally above the red curve when PSP is connected to a coronal hole (for instance between November 1st and November 14th), and below when crossing the current sheet (e.g. around November 15th). Interestingly, while the first model offers a better match with the data close to perihelion, the second works best after November 15th and PSP switching from one equatorial coronal hole (CH 1) to another (CH 2, see Figure 3 and Réville et al. 2020).

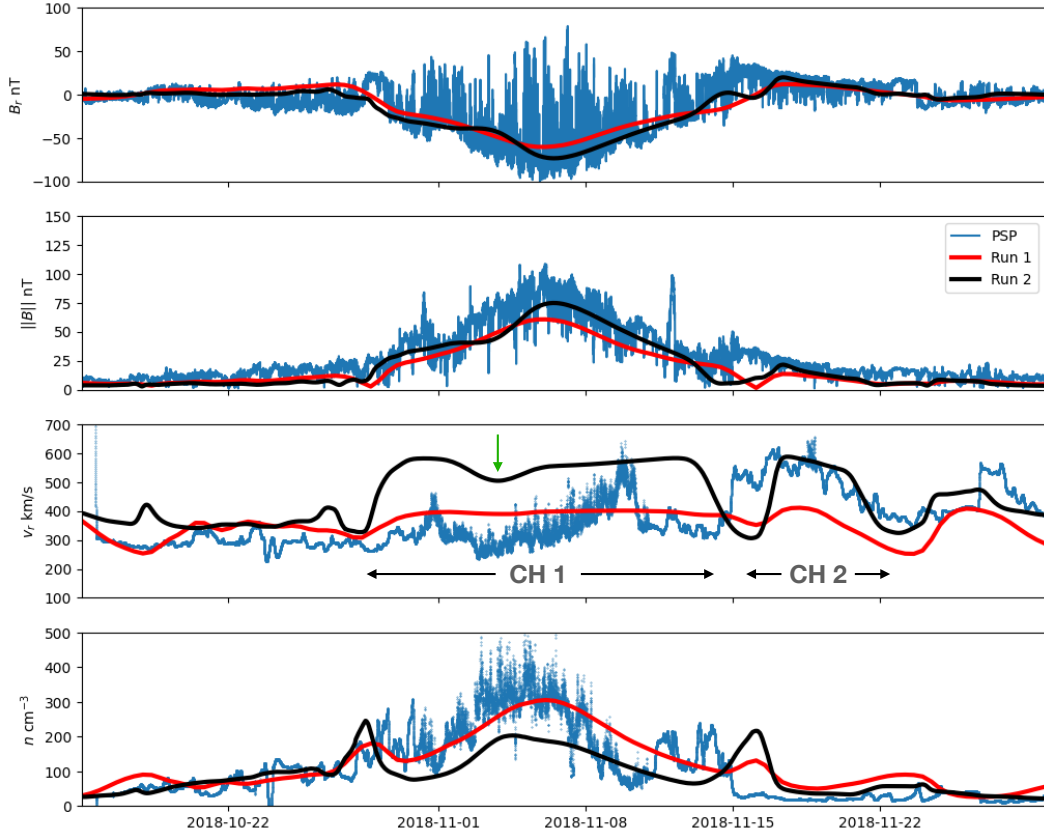


Fig. 2. Comparison of classical MHD quantities obtained along the trajectory of PSP in the simulations and the real data. Magnetic fields measurements (top and second panels) have been obtained thanks to the FIELDS instrument. Radial velocities and densities (third and fourth panels) are integrated moments of the Faraday cup (SWEAP/SPC).

The second model, however, shows speed variations inside the same coronal hole (green arrow in Figure 2), consistently with the data. This could be due to the higher resolution of Run 2, which allows to distinguish between the core and the boundary of the coronal hole at which PSP was connected. Note that both models have fast wind speed (≥ 600 km/s) above polar regions. Yet, in general, the solution with the transition region do provide more contrast and features in the simulated in situ data.

4 Remote sensing measurements

We now turn towards synthesized remote sensing measurements. More specifically, in the first row of Figure 3, we reproduce the UV emissions that would be measured by SDO/AIA with the 193 \AA channel. This filter yields information on the thermal structure of the solution in the low corona between 1 and 2 MK. First, we see the effect of the higher resolution. Although the same structures are visible, especially the coronal holes in dark, the image for Run 2 is smoother. The two coronal holes in the right (labelled CH 1 and CH 2) are the source of the plasma measured by PSP between November 1st and November 14th (CH 1) and after November 15th (CH 2). We note that both CH 1 and CH 2 are larger in Run 2 than in Run 1, which may explain the variation in the velocity observed in the data and better reproduced by Run 2.

More generally we see more contrast and stronger EUV emissions in Run 2. During PSP E1, a small active region has been emerging, and is identified in the synthetic measurements of Figure 3 by the AR 1 label. We note that the AR is visible in the synthetic measurements only for Run 2. The reason can be understood looking at the middle and bottom panels of Figure 3. We clearly see that, although the temperature is similar in both runs, there is an increased density at the active region in Run 2. The presence of the transition region provides the density reservoir necessary to the equilibrium of small magnetic loops. Hence, as noted in several

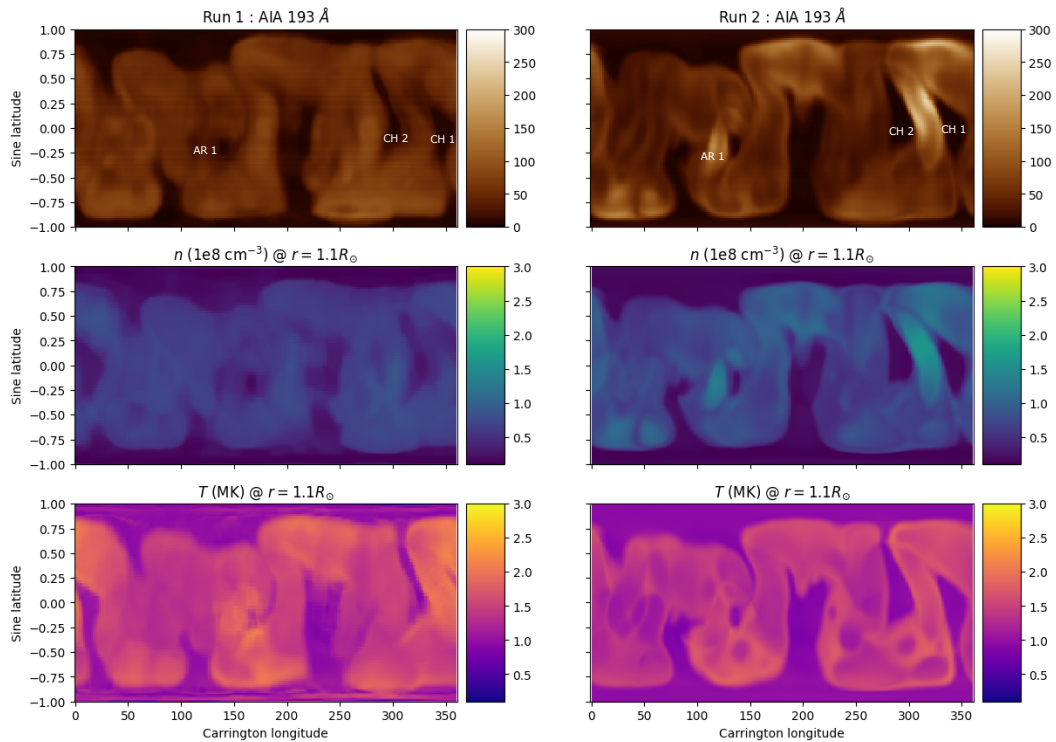


Fig. 3. Top panel: AIA 193 Å emission synoptic maps (integrated along the line of sight). Middle panel: synoptic map of the density at $1.1R_{\odot}$. Bottom panel: synoptic map of the temperature at $1.1R_{\odot}$.

previous investigations (see, e.g. Bradshaw & Cargill 2013; Cargill et al. 2015), the TR is essential to reproduce the thermal properties of active regions.

5 Conclusions

In these proceedings we have discussed the effect of adding a transition region in a global, Alfvén wave driven, coronal MHD model. The lowest layers of the solar atmosphere bring more contrast between the closed and open regions of the solar atmosphere and can in particular create a less dense and faster wind coming from equatorial coronal holes. The transition region is also essential to render correctly the density properties of small magnetic structures such as active regions as seen by EUV instruments such as SDO/AIA.

Numerical simulations have been supported by the GENCI program (grant A0090410293) and were made on Jean Zay machine (IDRIS). Parker Solar Probe was designed, built, and is now operated by the Johns Hopkins Applied Physics Laboratory as part of NASA’s Living with a Star (LWS) program (contract NNN06AA01C). This work utilizes data produced collaboratively between AFRL/ADAPT and NSO/NISP.

References

- Bradshaw, S. J. & Cargill, P. J. 2013, *ApJ*, 770, 12
 Cargill, P. J., Warren, H. P., & Bradshaw, S. J. 2015, *Philosophical Transactions of the Royal Society of London Series A*, 373, 20140260
 Downs, C., Lionello, R., Mikić, Z., Linker, J. A., & Velli, M. 2016, *ApJ*, 832, 180
 Lionello, R., Linker, J. A., & Mikić, Z. 2009, *ApJ*, 690, 902
 Réville, V., Velli, M., Panasenco, O., et al. 2020, *ApJS*, 246, 24
 Sokolov, I. V., van der Holst, B., Oran, R., et al. 2013, *ApJ*, 764, 23
 van der Holst, B., Sokolov, I. V., Meng, X., et al. 2014, *ApJ*, 782, 81